Interaction with human serum proteins reveals biocompatibility of phosphocholine-functionalized SPIONs and formation of albumin decorated nanoparticles

Irene Russo Krauss,[1,2,*] Alessandra Picariello,[1] Giuseppe Vitiello,[2,3] Augusta De Santis,[1,2] Alexandros Koutsioubas,[4] Judith E. Houston,[5] Giovanna Fragneto,[6] Luigi Paduano[1,2,*]

[1]Department of Chemical Sciences, University of Naples Federico II, Naples, Italy

[2] CSGI, Center for Colloid and Surface Science, Sesto Fiorentino (FI), Italy.

[3] Department of Chemical, Materials and Production Engineering, University of Naples Federico II, Naples, Italy

[4] Jülich Centre for Neutron Science (JCNS) at Heinz Maier-Leibnitz Zentrum (MLZ), Forschungszentrum Jülich GmbH, Lichtenbergstraße 1, 85747 Garching, Germany.

[5] European Spallation Source ERIC, Box 176, SE-22 100 Lund, Sweden

[6] Institut Laue-Langevin (ILL), 71 avenue des Martyrs, BP 156, 38042, Grenoble, France

*To whom correspondence should be addressed.

Irene Russo Krauss, Tel: +39 081674227; Email: irene.russokrauss@unina.it,

Luigi Paduano, Tel: +39 081674227; Email: luigi.paduano@unina.it

Abstract

Nanoparticles (NPs) are increasingly exploited as diagnostic and therapeutic devices in medicine. Among them, superparamagnetic nanoparticles (SPIONs) represent very promising tools for magnetic resonance imaging, local heaters for hyperthermia and nanoplatforms for multimodal imaging and theranostic. However, the use of NPs, including SPIONs, in medicine present several issues, first the encounter with the biological world and proteins in particular. Indeed, nanoparticles can suffer from protein adsorption, which can affect NP functionality and biocompatibility. In this respect, we have investigated the interaction of small SPIONs covered by an amphiphilic double layer of oleic acid/oleylamine and 1-octadecanoyl-*sn*-glycero-3-phosphocholine with two abundant human plasma proteins, human serum albumin (HSA) and human transferrin. By means of spectroscopic and scattering techniques, we analysed the effect of SPIONs on protein structure and the binding affinities, and only found strong binding in the case of HSA. In no case did SPIONs alter the protein structure significantly. We structurally characterized HSA/SPIONs complexes by means of light and neutron scattering, highlighting the formation of a monolayer of protein molecules on the NP surface. Their interaction with lipid bilayers mimicking biological membranes was investigated by means of neutron reflectivity. We show that HSA/SPIONs do not affect lipid bilayer features and could be further exploited as nanoplatform for future applications. Overall, our findings point towards a high biocompatibility of phosphocholine-decorated SPIONs and support their use in nanomedicine.

Introduction

Small particles with dimensions less than 100 nm are known as nanoparticles (NPs).[1] They are characterized by properties that are very different from those of both their constituent atoms/molecules and corresponding bulk materials because of their small size and large surface-to-volume ratio.[2] These unique NP properties are size-dependent, thus being in principle prone to be properly tuned,[1a] and cover a wide range of phenomena making them powerful tools to be used in a variety of fields including energy,[3] environment,[4] electronics,[5] biology[6] and biomedicine.[1b, 7] Concerning the last point, recent years have seen numerous innovations in using nanoparticles for medical imaging, novel therapeutic approaches and drug delivery.[7a, 7b, 8] The reasons of the impressive development of nanoparticles in medicine are various: i) as said nanoparticles possess unique physical and chemical properties, such as optical, magnetic, electrical, and electro-optical properties that can be exploited for both diagnosis and therapy; ii) they are small enough to interact directly with the cellular machinery and efficiently reach otherwise inaccessible targets; iii) they are optimally suited to be transported in the bloodstream and achieve good clearance.[9]

Among the NPs widely studied for biomedical applications, there are superparamagnetic iron oxide nanoparticles (SPIONs).[7b, 10] Probably the best-known application of SPIONs in nanomedicine is as Magnetic Resonance Imaging (MRI) contrast agent[10-11] and as local heaters for hyperthermia-based therapies.[12] However, they can be also used as nanoplatforms for multimodal imaging, for example by conjugation with optical imaging probes such as dye molecules, dye-doped silica materials, quantum dots, *etc*., or by adding a proper chelate molecule able to bind radioisotopes for PET applications;[13] as drug carriers, thus obtaining theranostic devices, realizing the need of real time monitoring of the therapy.[10a, 10d, 11]

Despite the great development of nanoparticles for biomedical uses, combining nanomaterials with biology presents several challenges.[14] The first issue to take into account is the stark contrast between the organic solvents in which nanomaterials are often produced and the complexity of common biological fluids, which are aqueous solutions with high salt and very high biomolecule concentrations.[9b]

The very first problem, i.e. facing the aqueous phase, can be overcome through a proper functionalization of the NP surface.[15] In this respect, some of us have developed an easy and versatile functionalization protocol based on hydrophobic interaction between the first layer of molecules that cover the NP surface exposing their apolar tails, as deriving from the synthesis step (i.e. oleic acid, oleylamine), and proper amphiphiles, such as phospholipids (for example 1-octadecanoyl-*sn*-glycero-3-phosphocholine, 18LPC). The resulting NP will present a double layer of amphiphiles and will be

soluble in water media. This strategy has been applied successfully to different metal NP, such as SPIONs[16] and Au NPs.[17] Moreover, as additional advantages, this approach does not involve any purification step and allow different functionalization to be performed by adding proper amphiphilic molecules, for example amphiphilic drugs[18] or target agents.[19]

As said before, biological fluids are not only based on water and salts, but also include thousands of different species, with a protein concentration greater than ~300 mg mL^{-1}. This is why biological environments often lead to unpredictable behaviour of inorganic materials.[20] Thus, the encounter with the complexity of the biological world, particularly proteins, is much more challenging than making NPs water-soluble. Nanomaterials can suffer from irreversible nonspecific adsorption and protein corona formation, the adsorption of proteins from the surrounding media onto the NP.[21] This can cause protein denaturation that can result in toxic effects and/or NP aggregation,[22,23] affect NP stability and induce aggregation with loss of NP function and possible toxic effects,[24] change the surface properties and alter the targeting ability of the NP.[20, 21b, 25]

In the last years, a great number of studies have investigated different aspects of formation and the consequences and utilization of the protein-corona in specific nanoparticle−protein systems. In particular, these studies can be broadly divided into three classes: (1) those focusing on the effect of nanoparticles on protein structure and properties; (2) those analysing the influence of protein molecules on nanoparticle stability and surface functionality; and (3) those investigating the behaviour of nanoparticle−protein composites in biological contexts.[26] In this respect, here we aim at presenting a thorough investigation of systems formed by SPIONs functionalized with 18LPC (hereafter simply SPIONs) and two abundant blood proteins, human transferrin (HTF) and human serum albumin (HSA). In particular, we analysed the effects of SPIONs on the protein secondary and tertiary structure, as well as protein thermal stability, by means of circular dichroism and fluorescence spectroscopy. Based on results indicating a significant binding only in the case of HSA-SPIONs, further confirmed by fluorescence quenching experiments, for this system we extended the study to include the effects of HSA on NP structure and stability, which were analysed by means of dynamic and electrophoretic light scattering, as well as small-angle neutron scattering. Finally, because as one of the concerns about these nano-objects in biological fluids is the lack of knowledge about how they interact with biologically relevant interfaces, specifically cell membranes,[27] we also investigated the behaviour of SPIONs/HSA with respect to lipid bilayers mimicking biological membranes.

Experimental

Materials

For the synthesis of nanoparticles, iron(III) acetylacetonate ($Fe(acac)_3$, purity grade 99%), 1,2-hexadecanediol (90%), oleylamine (70%), oleic acid (99%), diphenyl ether (99%), ethanol (98%) and cyclohexane (≥99.9%) were used as received from Sigma Aldrich. For the functionalization step 1-stearoyl-2-hydroxy-3glicerno-sn-phosphocholine (18LPC >99%) was purchased from AvantiPolar Lipids Inc. The proteins human serum albumin (HSA) and apo-human transferrin (HTF) were purchased from Sigma Aldrich. HSA was fatty acid free and globulin free, with a purity grade ≥99%, HTF has a a purity grade ≥98% and an iron content ≤0.005%.

SPION synthesis and functionalization

SPIONs were synthesized as previously reported through a modified version of the thermal-decomposition method:[28] namely iron(III) acetylacetonate, oleylamine, oleic acid and diphenyl ether were mixed together in a three-neck flask, the solution was heated at 100 °C under argon atmosphere and vigorous stirring. Then 1,2-hexadecanediol and another aliquot of diphenyl ether were added to the flask and kept at 200 °C for 30 min. For the last 90 min, the temperature was increased to 280°C. At the end of the synthesis, the suspension was washed with cold ethanol and centrifuged at 6000 rpm for 20 min, twice. SPIONs are thus obtained as a dark brown solid precipitate, which is gradually dispersed in hexane. The iron concentration in the final product was evaluated by means of Inductively Coupled Plasma Mass Spectrometry.[16, 18a]

By considering nanoparticle dimension and Fe_3O_4 density, starting from Fe concentration we evaluated an indicative nanoparticle molar concentration as described in the supplementary information.

Nanoparticles were functionalized through a stratification protocol, i.e. the suspension of SPIONs in hexane was stratified over an aqueous solution of 1-octadecanoyl-sn-glycero-3-phosphocholine (18LPC) at a SPIONs/18LPC molar ratio of 1:1000, and sonicated in an ultrasound thermostat bath at 50 °C. After about 2 h, a clear brown water dispersion of nanoparticles, covered with a bilayer of oleic acid/oleylamine and 18LPC, is obtained.[16, 18a] The resulting functionalized nanoparticle solutions have concentration of about 1 mg ml^{-1}, expressed as Fe concentration, corresponding to about 10^{-6} M NP concentration. Hereafter nanoparticles coated with 18LPC are simply called SPIONs.

SPIONs were extensively characterized by some of us,[16, 18a] while here we have reported DLS and ELS analysis for comparison with NP-protein systems.

Protein-SPIONs samples

Stock solutions of protein have been prepared by dissolving them in either phosphate buffered saline solution (PBS) or 10 mM sodium phosphate buffer at pH 7. Each protein sample was filtered on 0.2 μm filter in order to remove impurity and then protein concentration was determined by means of UV spectroscopy at 280 nm. Protein-SPIONs samples were prepared by proper mixing of stock solutions in order to achieve the desired NP-protein molar ratio, 1:50, 1:100 in order to mimic the average concentration ratio expected to be used in *in vivo* applications,[18a] and the protein concentration necessary for the experimental technique used, or the increasing ratios required by fluorescence quenching experiments. Resulting solutions were either used with no further treatment or extensively washed to remove excess protein. In the latter case we used a Centricon mini-concentrator with a vertical membrane and cut-off 100 KDa (Millipore) and performed several washing steps by centrifugation at 20 °C and 10000 x g. At each step, the washing waters were removed from the bottom of the Centricon and an equal volume of buffer solution was added to the protein/NP sample in the Centricon in order to keep the concentration of the sample constant.

Circular dichroism

Circular dichroism (CD) spectra were recorded at 20 °C using a Jasco J-715 spectropolarimeter equipped with a Peltier thermostatic cell holder (Model PTC-348WI). CD measurements were carried out in the 260–200 nm range, using a 0.1 cm path length cell and solutions at 0.2 mg ml^{-1} protein concentration in either PBS or 10 mM Na-phosphate buffer at pH 7, with 0.5 nm data pitch, 2 nm band width and 20 nm min^{-1} scanning speed. The same conditions were employed in the case of both free proteins and proteins incubated with SPIONs. Thermal unfolding curves were obtained by following the CD signal at 222 nm in the 10 – 90 °C range, at heating rate of 1.0 °C min^{-1}.

The unfolded fraction was calculated as

$$f = \frac{I_x - I_0}{I_f - I_0} \qquad \text{Eq. 1}$$

where f is the denatured fraction, I_x is the CD intensity at 222 nm at the temperature T, and I_0 and I_f are the intensity at the lowest temperature and at the highest temperature, respectively. We plotted f as a function of T and calculated melting temperatures by fitting the experimental data with a sigmoidal function.

Fluorescence spectroscopy

Fluorescence spectra were recorded at 20 °C using a Horiba Scientific Fluoromax-4 spectrofluorometer equipped with a Peltier control system and 1 cm path length cells. The same solutions at 0.2 mg mL^{-1} protein concentration and 1:50 or 1:100 NP:protein ratio that were analysed by means of CD spectroscopy were employed for fluorescence spectroscopy. Tryptophan residues were selectively excited at 295 nm, whereas both tyrosine and tryptophan residues were excited at 280 nm; in the former case the investigated emission range was 295-500 nm, and in the latter 310-500 nm. Both excitation and emission slit widths were set to 5 nm.

The interaction between proteins and SPIONs was monitored by means of fluorescence quenching experiments, by preparing nanoparticle-protein solutions at fixed protein concentration, optimized to have the maximum fluorescence intensity, and increasing the nanoparticle concentration in the nanoparticle-protein molar ratio 1:100-1:20 range with a 10-fold increase of NP content from one sample to the other, i.e. we analysed samples with 1:100, 1:90, 1:80 and so on protein-NP molar ratios. Each solution was incubated for 2 h before measurements.

First analysis of quenching data was performed by means of Stern-Volmer plot: the ratio between the fluorescence intensity in the absence of quencher, F_0, and that in the presence of quencher, F, was plotted as a function of the quencher (i.e. SPIONs) concentration. In the case of HSA a straight line was obtained, allowing the Stern-Volmer constant K_{sv} to be determined through

$$\frac{F_0}{F} = 1 + K_{SV}[SPIONs] = 1 + K_q\tau_0 \qquad \text{Eq. 2}$$

where τ_0 is the mean fluorescence lifetime of the fluorophore (HSA) and K_q is the quenching efficiency. The calculated K_q value allowed us to distinguish between static and dynamic quenching phenomena, with the former characterized by K_q greater and the latter smaller than 2×10^{10} $M^{-1}s^{-1}$.[20, 29]

In the presence of static quenching, data can be also treated by modified Stern-Volmer analysis, by plotting $log\frac{F_0-F}{F}$ as a function of $log\ [quencher]$ and employing

$$log\frac{F_0-F}{F} = log\,K_a + nlog\,[SPIONs] \qquad \text{Eq. 3}$$

it is possible to determine the binding constant, K_a, from the intercept, and the number of quencher binding sites, n, from the slope of the straight line.[20, 30]

Dynamic light scattering

The dimensions of SPIONs/protein assemblies, and of isolated proteins and nanoparticles for comparison, as well as the possible formation of aggregates were evaluated by dynamic light

scattering (DLS). DLS measurements were performed on a homemade instrument composed of a Photocor compact goniometer, a SMD 6000 Laser Quantum 50 mW light source operating at 5325 Å, a photomultiplier (PMT-120-OP/B) and a correlator (Flex02−01D) from Correlator.com. The experiments were carried out at 25.0 °C, keeping the temperature constant by a thermostatic bath, and at a scattering angle θ = 90°. For DLS analysis 10 or 20 mg mL^{-1} protein samples were used, while SPIONs concentration was about 1 mg mL^{-1}. The scattered intensity correlation function was analysed using a regularization algorithm.[31] The diffusion coefficient of each population of diffusing particles was calculated as the Z-average of the diffusion coefficients of the corresponding distributions. Being all the samples diluted solutions, the Stokes−Einstein equation was used to evaluate the hydrodynamic radius, R_H, from translation diffusion coefficients, D.[31]

Electrophoretic light scattering

Surface charge (zeta potential) of SPIONs, proteins and SPIONs/protein assemblies was evaluated by means of electrophoretic light scattering using a Zetasizer Nano ZSP (Malvern Instruments, England). All the measurements were performed using 10 mg mL^{-1} protein or protein/SPION solutions and 1 mg mL^{-1} SPION solutions in 10 mM sodium phosphate buffer pH 7.4, previously filtered with 220 nm cut-off microfilters, and polystyrene Folded Capillary Zeta cells (Malvern Instruments). Each measurement was performed at 25 °C upon 30 s equilibration time, the average of three measurements at stationary level has been taken. Zeta potential was calculated by applying the Smoluchowski model.

Small-angle neutron scattering

Small-angle neutron scattering (SANS) measurements were performed at 25 °C on the KWS-2 diffractometer operated by Julich Centre for Neutron Science at the Heinz Maier Leibnitz Zentrum, Garching (Germany).[32] For both HSA (30 mg mL^{-1} protein concentration) and SPIONs/HSA (10 mg mL^{-1} NP concentration incubated with HSA in a 1:50 NP:protein ration and then purified to remove protein excess) samples, an incident wavelength of 5 Å and wavelength spread of $\Delta\lambda/\lambda \leq 0.1$ were used. A two-dimensional array detector at three different wavelength (W)/collimation (C)/sample-to-detector (D) distance combinations (W 5 Å/C 8 m/D 2m; W5 Å/C 8 m/D 8m; and W5 Å/C 20 m/D 20 m) measured neutrons scattered from the samples. These configurations covered a q range from 0.08 $Å^{-1}$ to 0.4 $Å^{-1}$. The raw data were corrected for background and empty cell scattering. The absolute scattering cross section $d\Sigma/d\Omega$ data were plotted as a function of the scattering vector q obtaining a scattering profile. The dependence of $d\Sigma/d\Omega$ from the scattering vector can be summarized as

$$\frac{d\Sigma}{d\Omega} = \Phi_P V_P P(q) S(q) + bkg \qquad \text{Eq. 4}$$

where ϕ_p and V_p represent the volume fraction of the particles and the particle volume, respectively, *P(q)* and *S(q)* are the form and the structure factor of the scattering particles, and *bkg* is the incoherent and inelastic part of the scattered cross section, largely dependent on any hydrogen present. The form factor is responsible for the shape, size, and size distribution of the scattering particles, while a contribution of the structure factor can be considered when an interparticle correlation exists. Experimental data were fitted with an appropriate model by using SASview program (SasView 4.0.1software, https://www.sasview.org/) in order to get structural information contained in the form factor.

Neutron reflectivity

Neutron reflectivity experiments aiming at investigating the interaction between model membranes and SPIONs/HSA were performed at 25 °C with the MARIA Reflectometer operated by Julich Centre for Neutron Science at the Heinz Maier Leibnitz Zentrum, Garching (Germany)[33] and D17 reflectometer operating at Institute Laue Langevin (ILL), Grenoble, France.[34]

We used bilayers with two different lipid compositions, namely 1-palmitoyl-2-oleoyl-sn-glycero-3-phosphocholine/1-palmitoyl-2-oleoyl-sn-glycero-3-(phospho-rac-(1-glycerol))/cholesterol (POPC/POPG/Chol) 72:8:20 and 54:6:40 mol/mol/mol as model membranes. Each bilayer was characterized before and after addition of SPIONs/HSA solutions at 1 mg/ml iron concentration, in three different contrast media, H_2O, D_2O and silicon match water (SMW). NR profiles were fitted to a box model using the Aurore software[35] and characterizing each box by its thickness, scattering length density (*sld*), solvent volume fraction and interfacial roughness. The first two boxes correspond to the silicon block and the thin solvent layer interposed between it and the supported bilayer; the remaining three boxes describe the lipid bilayer, namely the inner headgroups, the hydrophobic chains and the outer headgroups. In the case of systems containing HSA or SPIONs/HSA, an additional layer was taken into account.

Results and discussion

Effect of NPs on HTF and HSA structure

The first indication of the effect of NPs on serum proteins human transferrin (HTF) and human serum albumin (HSA) was obtained by comparing the CD spectra of HTF and HSA incubated with NP in two different NP:protein molar ratios, 1:100 and 1:50, with those of the corresponding pure protein in PBS (Figure 1). This is possible because CD spectra of SPIONs are featureless and with near-zero intensity (data not shown), thus they do not affect CD spectra of proteins. NP:protein samples were

used with no further purification, i.e. in the presence of excess protein. In the case of NP:HTF 1:100, the spectrum is completely superimposable with that of pure protein, with two minima at about 208 and 222 nm and a maximum below 200 nm (Figure 1A), in good agreement with the predominantly α-helicoidal structure of this protein.[36] At the higher NP:protein ratio, only a very slight change of intensity is observed (Figure 1B), pointing towards no significant change of transferrin secondary structure induced by the presence of NPs.

In the case of HSA, a slight change of CD spectrum is observed in the NP:HSA 1:100 system, in particular the minimum at $\lambda \approx 222$ nm is less intense than that found for pure HSA (Figure 1C). At NP:protein 1:50 ratio, intensity of CD spectrum further decreases with respect to pure protein, but the shape is essentially the same (Figure 1D). These findings point towards an interaction between human serum albumin and NPs. Moreover, slight change in CD may arise from protein molecules that have been sitting on the NP surface and desorb with slightly different confirmation.

However, NPs even affecting protein structure do not cause unfolding or dramatic changes of secondary structure.

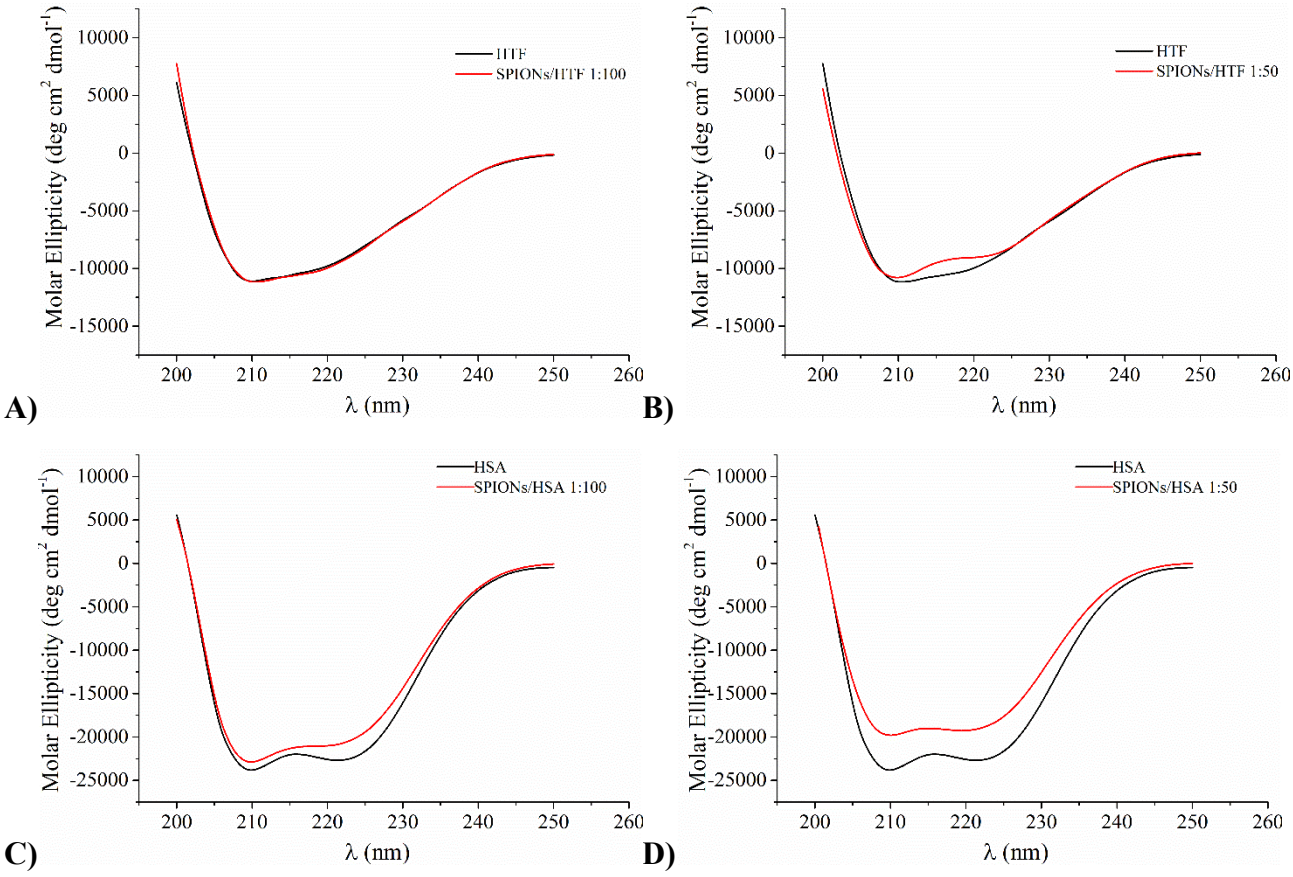

Figure 1 Comparison of far UV CD spectra of HTF (panels A and B) and HSA (panels C and D) incubated in the presence of SPIONs at two different NP:protein molar ratios (1:100 panels A and C, 1:50 panels B and D) with respect to spectra of pure proteins.

All NP-protein samples were analysed for 48 h, with the aim at revealing any change induced by long incubation times. In the case of HTF, no change is observed at both 1:50 and 1:100 ratios (Figure 2 A and B), while for HSA, at both NP:protein ratios, a slight intensity decrease occurs in the first 24 h, but no further change was observed in the following hours (Figure 2 C and D). Significantly, no precipitation or change in the appearance of the solution was detected in any case.

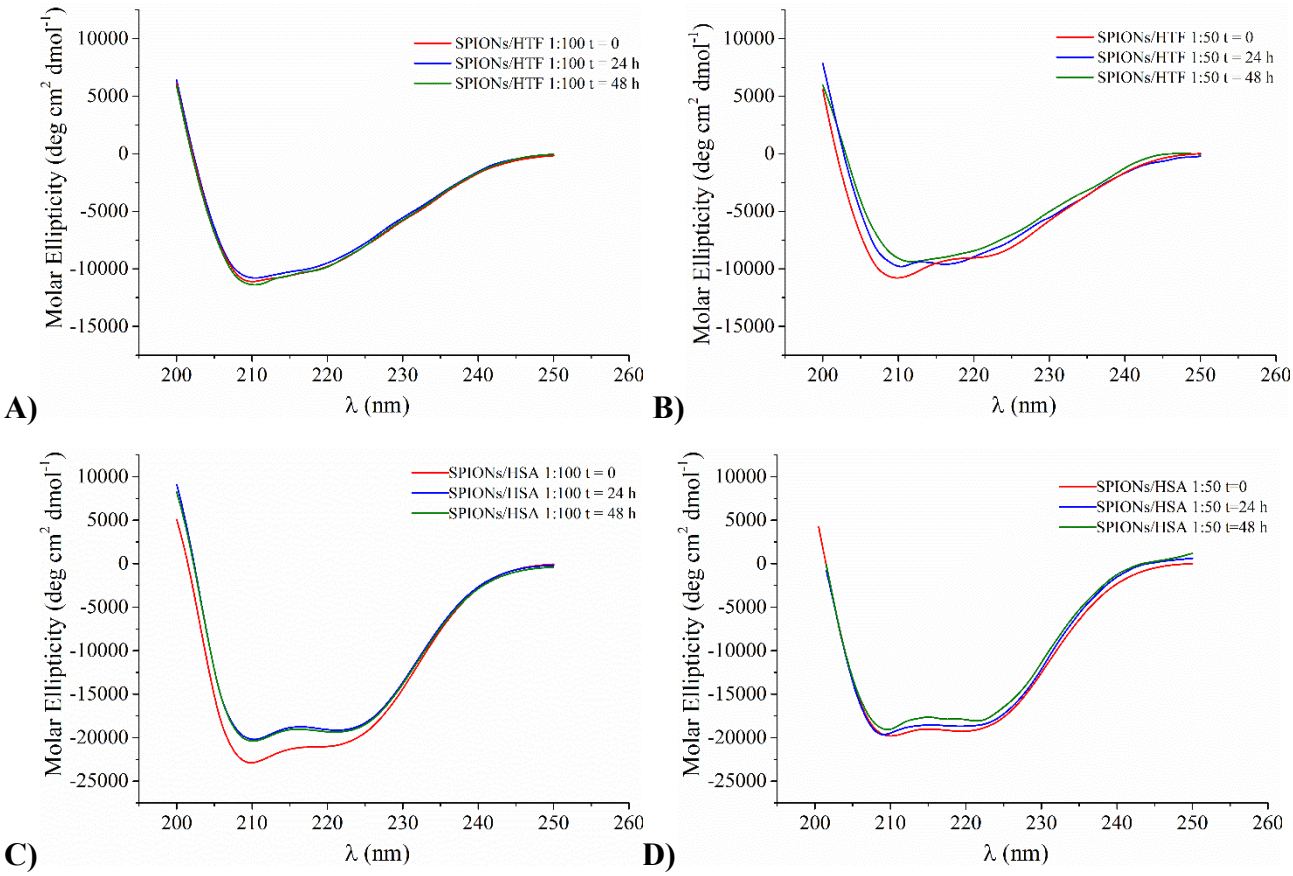

Figure 2 Time evolution of far UV CD spectra of HTF (panels A and B) and HSA (panels C and D) incubated in the presence of SPIONs at two different NP:protein molar ratios (1:100 panels A and C, 1:50 panels B and D) during two days observation.

The effects of NP on the protein tertiary structure were investigated by means of fluorescence spectroscopy for samples with NP:protein molar ratio 1:100 or 1:50. In the former case, no change is observed with the exception of a decrease in fluorescence intensity with both HTF and HSA (data not shown), with SPIONs acting as quenchers of protein fluorescence. At NP:protein molar ratio 1:50, in the case of HTF the presence of NP does not induce any shift of emission maximum, neither with excitation wavelength 280 nm nor 295 nm (Figure S1), indicating that environment of aromatic

residues is not affected at all by the presence of NPs. In the case of HSA, no shift is observed for spectra obtained with excitation wavelength 280 nm, while a blue shift (about 4 nm) is found with λ_{ex} = 295 nm (Figure 3), indicating that the only tryptophan residue of HSA experiences a more apolar environment with respect to HSA alone, probably due to interaction with NPs.

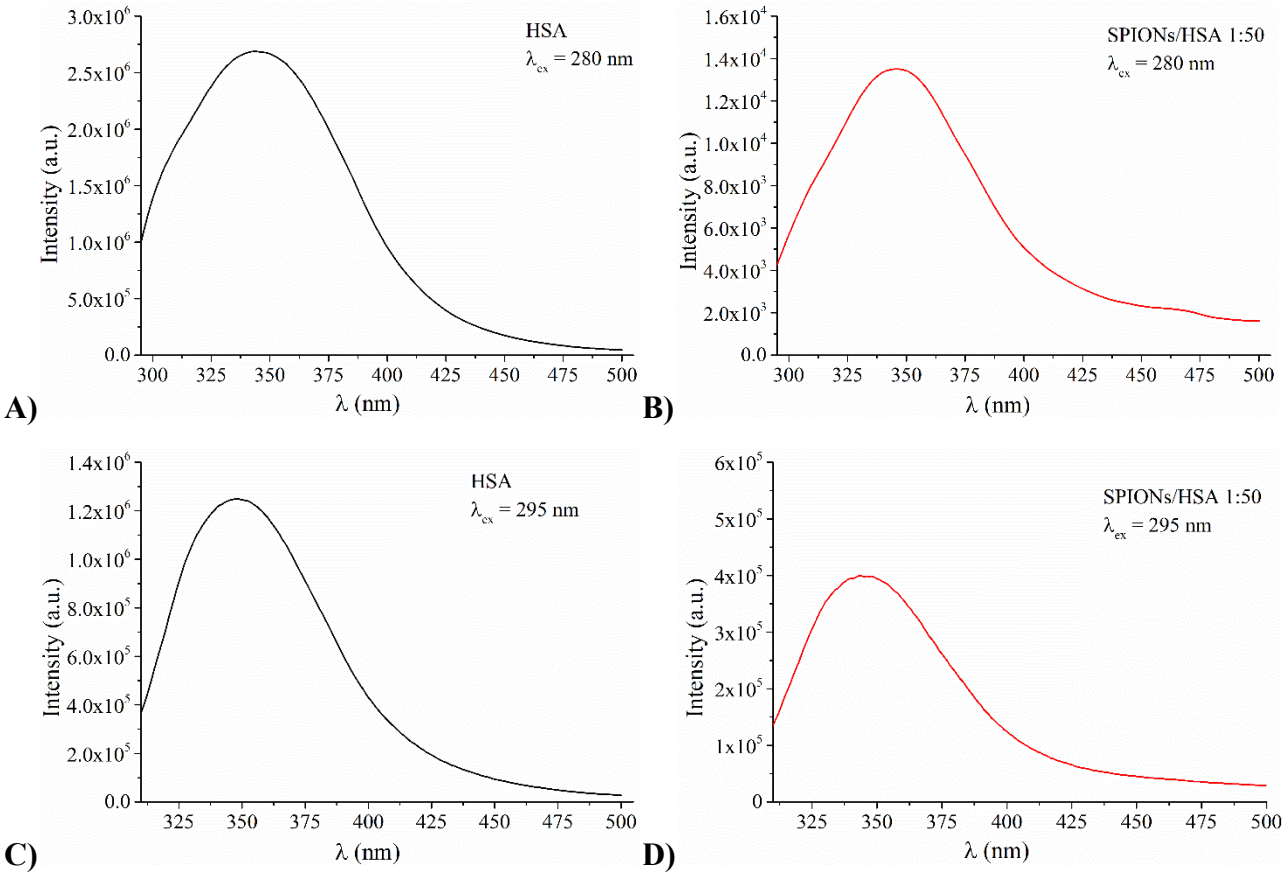

Figure 3 Fluorescence spectra of HSA in the absence (panel A and C) and in the presence of SPIONs at NP:protein molar ratio 1:50 (panel B and D) obtained by exciting at either λ_{ex} = 280 nm (panels A and B) or λ_{ex} = 295 nm (panels C and D).

At 1:50 NP:protein ratio the quenching of protein fluorescence is even more marked (see also Figure S2 where spectra of Figure 3 have been overlapped) suggesting a NP concentration-dependent phenomenon.

The very small change of fluorescence spectra does not seem consistent with any change of protein tertiary structure: SPIONs do not cause significant change of protein secondary and tertiary structure for both HTF and HSA.

Interestingly, when incubated in 18LPC solutions, a significant blue shift of maximum fluorescence wavelength occurs in SPIONs/HSA systems (Figure S2). An about 10 nm blue shift in the case of

excitation at both 280 and 295 nm indicates that aromatic residues experience a more apolar environment, likely due to extensive binding of 18LPC, which should be in part hindered when it is closely packed on SPION surface.

Effect of NPs on HTF and HSA structure stability

With the aim at investigating whether NPs can alter protein stability, and assessing a HTF-NP interaction not immediately evident from comparison of CD spectra, we performed thermal unfolding experiments for different samples and compared melting profiles and melting temperatures with those of pure proteins. In particular, CD signal at 222 nm was followed in the 10 – 90 °C range, and the corresponding CD signal was used to calculate the unfolded fraction.

Melting profiles for HTF and HSA, alone and incubated with NP at two different NP:protein molar ratios, are reported in Figure 4 A and B, respectively. All melting profiles present a sigmoidal shape that is not affected by the presence of NPs, indicating a mostly cooperative unfolding. In the case of HTF the three curves are perfectly superimposable, with no effect of NP; in contrast, in the case of HSA a slight shift towards higher temperatures is observed for both NP:HSA systems, with a Tm=69°C and Tm=73°C for HSA and NP:HSA, respectively.

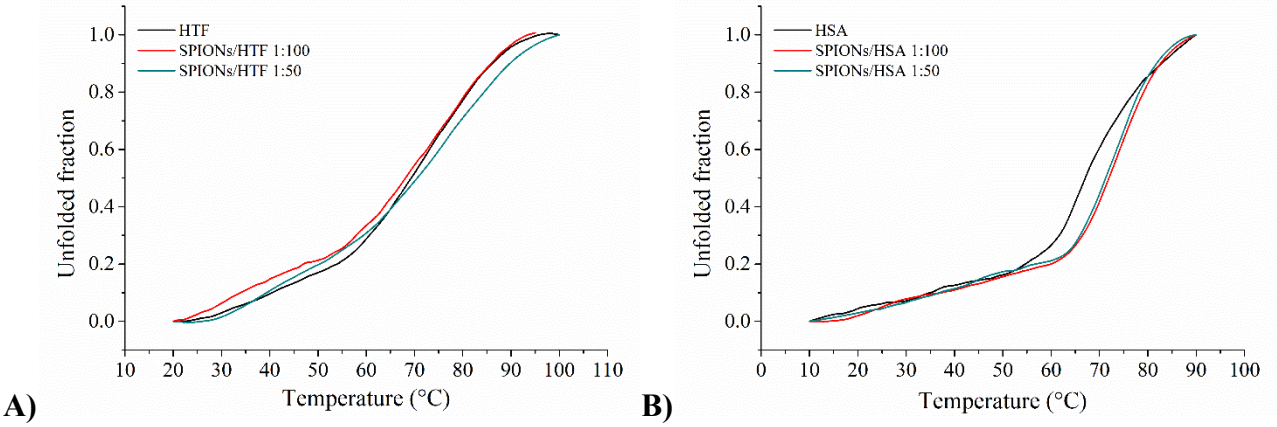

Figure 4 Melting profiles of HTF (panel A) and HSA (panel B) alone and incubated in the presence of SPIONs at 1:100 and 1:50 NP:protein molar ratios, as derived from analysis of CD spectra in the 10-90°C temperature range.

No melting profile change was observed in the following two days (as an example see SPIONs/HSA 1:50 in supplementary material Figure S3).

Overall CD analysis points toward a NP:HSA interaction, resulting in a slight change of protein structure, which is more stable with respect to temperature than native HSA structure. In contrast, no

indication of a HTF-NP interaction arises: either NP do not affect any of HTF properties or they do not interact at all.

When comparing CD spectra and thermal profiles of HSA in the presence of 18LPC and HSA alone (Figure S5), no significant difference is observed. Thus, even if some residual 18LPC were present in nanoparticle samples, the different behaviour of the protein in the presence of NPs and in the presence of 18LPC seems to indicate that HSA interacts mainly with NPs in these samples.

Insights into SPIONs/protein recognition

Fluorescence spectra of proteins in the presence of SPIONs have revealed that nanoparticles act as quenchers of protein fluorescence, and this behaviour can be used to get information on the binding process, in particular to estimate the binding constant. Indeed fluorescence quenching was shown to be a convenient method to investigate NP-protein interactions, giving results consistent with those obtained by ITC,[21a] and this is particularly true for protein containing exposed aromatic residues. HSA has only one Trp, not buried in the inner core of the protein, but located in a superficial pocket accessible to the solvent, as highlighted by the λ_{max} = 348 nm that is about 15 nm red shifted with respect to typical values of buried Trp residues, and to ligand binding.

We acquired fluorescence spectra at fixed protein concentration and increasing SPION concentration (Figure S6). Data were elaborated through the Stern-Volmer analysis, by plotting the ratio between the protein fluorescence intensity with no quencher (F_0) and the observed fluorescence in the presence of quencher (F) as a function of the quencher concentration. In the case of HSA experimental data fall on a straight line (Figure 5A) that was fitted according to Eq. 2

$$\frac{F_0}{F} = 1 + K_{SV}[SPIONs] = 1 + K_q\tau_0 \qquad \text{Eq. 2}$$

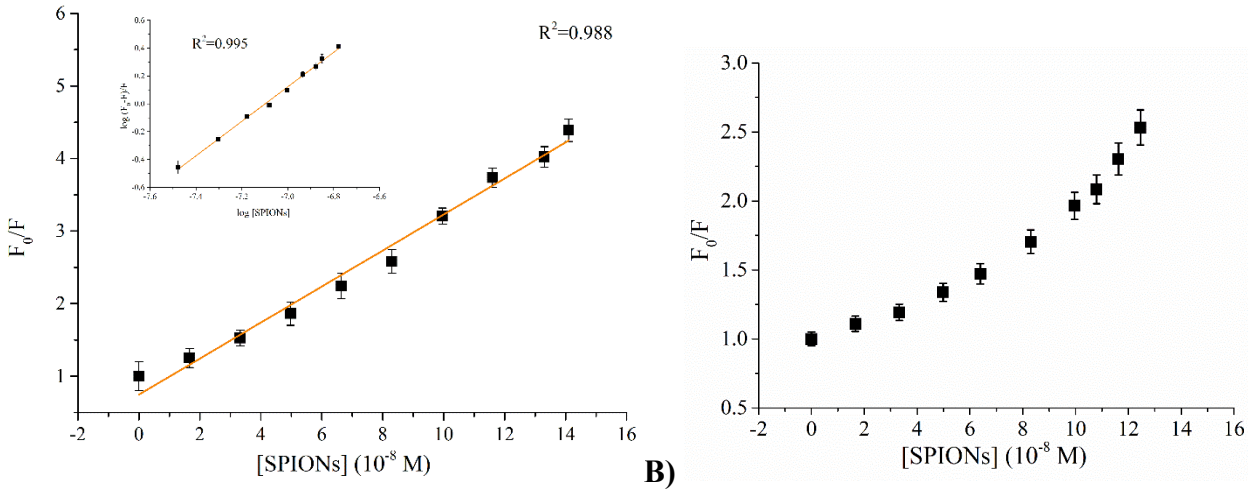

Figure 5 Stern-Volmer plots determined for SPIONs/HSA (A) and SPIONs/HTF (B) systems at fixed protein concentration and increasing NP concentration. λ_{exc} = 295 nm. For SPIONs/HSA modified Stern-Volmer is reported in the inset of panel A

From the slope we determined a Stern-Volmer constant value K_{SV} = 2.5×10^7 M^{-1}, by knowing the mean fluorescence lifetime of HSA τ_0= 7.1×10^{-9} s, as reported in the literature,[37] a quenching efficiency K_q = 3.8×10^{15} M^{-1} s^{-1} results. Quenching mechanisms can be distinguished in static and dynamic, depending on the K_q value. The static mechanism implies the formation of a protein–quencher complex stabilized by a strong interaction, whereas dynamic quenching implies a weak interaction between the protein and the quencher. The K_q value (3.8×10^{15} M^{-1} s^{-1}) acquired here is exceptionally larger than the maximum diffusion-controlled bio-molecular rate constant, and such observation indicates that we can confidently consider a static quenching occurring,[38] pointing towards the formation of a stable HSA/SPION complex.

Being in the presence of static quenching, we analysed data through a modified Stern-Volmer plot, by reporting $log\ \frac{(F_0-F)}{F}$ as a function of *log [SPIONs]* (Inset of Figure 5A) in order to calculate the binding constant K_a and the number of binding sites on the fluorophore (i.e. HSA) n, by means of Eq. 3

$$log\frac{(F_0-F)}{F} = logK_a + nlog[SPIONs] \qquad \text{Eq. 3}$$

We determined n = 1.2, indicating that there is only one kind of binding site for HSA binding on SPION surface. For what concerns the binding constant, we determine K_a = 6.2 × 10^8 M^{-1}. This value is higher than that found for binding of bovine serum albumin, a protein highly homologue to HSA,

to other SPIONs with different coating layers,[20, 39] confirming the importance of the coating molecules in determining NP properties.

In the case of HTF the plot of F_0/F as a function of SPIONs concentration does not describe a linear trend but have an exponential growth (Figure 5B), which is an index of the likely coexistence of both static and dynamic quenching phenomena. Thus, it can be inferred that a slight interaction between SPIONs and HTF occurs, but not significant as that observed for the HSA system. The interaction between NP and HTF is corroborated by dynamic light scattering analyses of SPIONs/HTF 1:100 and comparison with reference systems, i.e. isolated SPIONs and HTF. Isolated systems present a single peak indicating a monodispersed solution, with R_H equal to 8±1 and 5±1 nm for SPIONs and HTF, respectively. On the other hand, the SPIONs/HTF 1:100 system always presents a population due to the protein excess and a larger population, whose dimension changes from sample to sample and ranges between 20 and 40 nm (see Figure S7A). In the following two days of observation, large polydisperse aggregates formed (Figure S7B) as a result of further protein-mediated interactions or depletion effects.

Characterization of SPIONs/HSA assemblies

To get further insights on SPIONs/HSA assemblies, in particular on their nature and stability, considering the strong binding between the protein and the NP surface highlighted by the K_a value, we also analysed SPIONs/HSA samples where the excess protein was washed away by using a Centricon mini-concentrator with 100 KDa cut-off. Once excess HSA was washed away, the SPIONs/HSA samples were analysed by means of circular dichroism, dynamic and electrophoretic light scattering, as well as small-angle neutron scattering.

After extensive washing, CD spectra of NP/protein samples show a marked decrease of overall intensity, coherently with a reduction of protein concentration due to removal of HSA excess (Figure S8). However, they retain all the spectral features of HSA, i.e. the double minima at 222 and 208 nm and the maximum at 190 nm, and once normalized they are fully superimposable with those of the same systems before washing (Figure 6) (uncertainty on protein concentration does not allow a straight comparison of spectra without normalization). These findings prove not only that a significant fraction of HSA molecules is stably bound on NP surface, but also that they are indeed well-structured folded protein molecules.

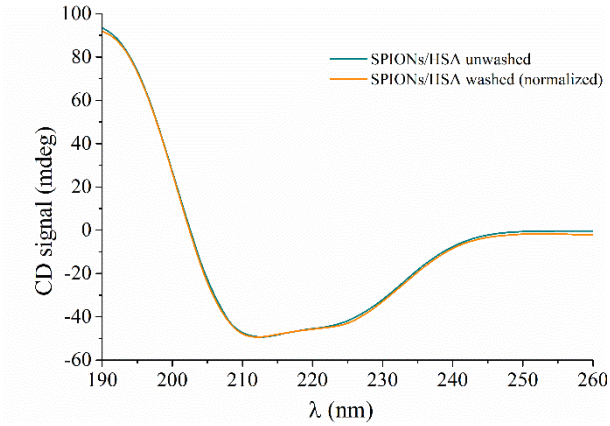

Figure 6 Comparison of normalized CD spectra for SPIONs/HSA system before (unwashed) and after (washed) removal of protein excess.

As a control, when the same procedure was applied to SPIONs/HTF samples, almost the entire protein was recovered in the washings, since CD spectra of washed SPIONs/HTF were featureless (data not shown), proving that HTF does not firmly bind NPs.

SPIONs/HSA systems were further characterized by means of dynamic light scattering. Determination of hydrodynamic radius (R_H) of SPIONs in the presence of HSA allows the formation of either a protein corona or NP-protein aggregates to be detected. With this aim, we characterised the different systems, the isolated protein and nanoparticles, and the protein/nanoparticles system. Analysis of isolated HSA shows the presence of a monodispersed species with R_H 4±1 nm, and, similarly to what happens to SPION sample, it does not change with time. In the washed SPIONs/HSA system, upon removal of excess HSA, a single main population is present, characterized by a hydrodynamic radius higher than those of the isolated protein and nanoparticles (R_H = 11±1) (Figure 7A). It is interesting that DLS analysis of SPIONs/HSA 1:100 before washing highlights the presence not only of the excess protein, but also of a population larger than that observed in the washed system with R_H = 25±3 nm. This population may be due to SPIONs/HSA aggregates or to formation of multiple HSA layers on NP surface. The latter hypothesis should indicate a behaviour different from that of BSA and other SPIONs.[20] However, even considering the possible binding of HSA in multiple layers, only the first one is firmly anchored on NP surface and is not removed by washing suggesting formation of a hard and a soft corona of HSA.

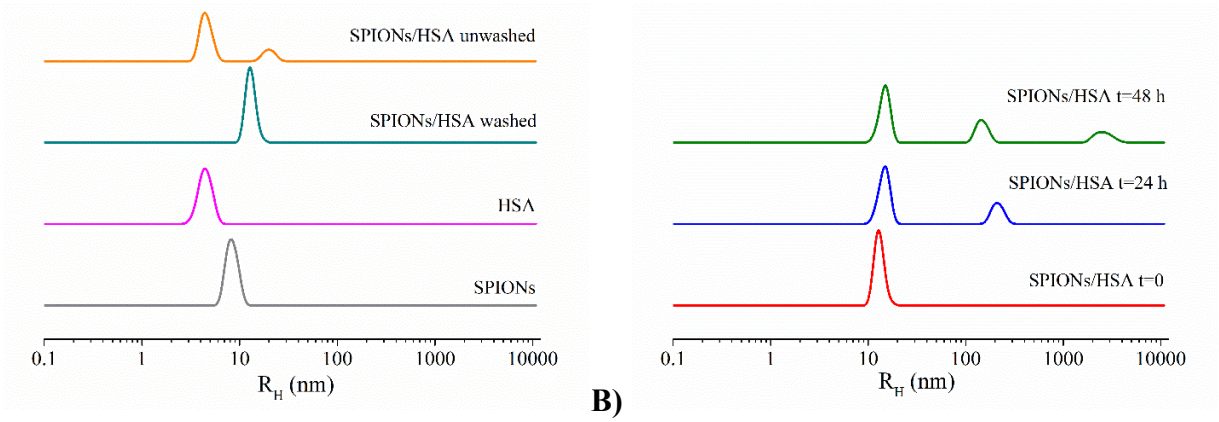

Figure 7 DLS profiles of SPIONs/HSA with respect to isolated NP and protein (panel A); time evolution of DLS profiles of SPIONs/HSA during two days observation (panel B)

In the following two days, we observe formation of new populations: the main population can always be ascribed to the mixed NP/protein aggregates, even if larger aggregates are also visible (Figure 7B).

The SPIONs/HSA system was characterized by means of electrophoretic light scattering to determine the surface charge of the aggregates in terms of Z-potential. Measurements were performed in phosphate buffer, in order to avoid any interference due to the salts present in PBS. Before the analysis, CD spectra were recorded to assess that the change of buffer does not alter protein structural features (data not shown). For comparison, we analysed isolated components as well (Figure 8).

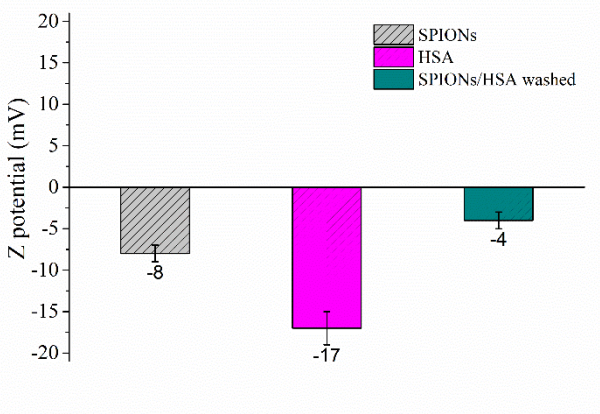

Figure 8 Comparison of zeta potential values for SPIONs/HSA after removal of protein excess with respect to those of isolated NPs and protein.

SPIONs and HSA are both characterized by negative values of Z potential, indicating that they have the same net charge. However, several studies showed that the binding to negatively charged NP is not enhanced for proteins that were overall positively charged at pH 7.4. This happens because

considering the Debye length at the typical ionic strengths of PBS buffer (and biological fluids), which is <1 nm and thus smaller than the size of a protein, coulombic interactions are essentially only effective between charges located on the NP and protein surfaces that are in close contact.[40] Patches with different net charge are indeed present on the HSA surface and they may mediate its interaction with SPION surface, as reported for other NP/protein systems.[41] SPIONs/HSA also present a negative Z potential, but with a completely different value with respect to isolated components, in particular we observe a drop of zeta potential. This decrease can be attributed to the screening of NP and protein negative charges due to their reciprocal interaction.

Incidentally, it should be noted that the low absolute value of Z potential determined for SPIONs/HSA system may be an index of a reduced stability of the species in solution, which in turn justifies the formation of big aggregates observed in DLS profiles at long incubation times as some sort of aggregated SPIONs coated with HSA.

Finally, aiming at getting a deeper insight into the structural features of SPIONs/HSA aggregates, we employed SANS, which allows us to determine the shape of these aggregates and the thickness of the protein layer that likely coats the NPs.

The SANS profile of SPIONs/HSA upon removal of excess protein is reported in Figure 9 (SANS profile of HSA is reported in Figure S9). This scattering intensity profile is typical of nanoparticles, where the scattering length densities (*sld*) of the core and the solvent are almost matched. Furthermore, the system is characterized by some polydispersity that smooths oscillation in the scattering profiles. The slight slope of q^{-1} at low q suggests small nanoparticles clustering, which could be expected since the sample was analysed a few days after purification and DLS already showed aggregate formation with time (Figure 7B). Experimental data were fitted using a core–shell sphere model (black line in Figure 9), with the Fe_3O_4 representing the core and the organic layers, including oleic acid/oleylamine, 18LPC and the newly added protein, representing the shell, and a power law to take into account the raise at low-q due to the presence of aggregated species. A Shultz polydispersity of the size of the NPs has been taken into account, resulting in a polydispersity index of about 0.6. The absence of any peak in the scattering profile indicates that the nanoparticles can be considered as non-interacting objects and a structure factor does not need to be included in the fitting procedure.

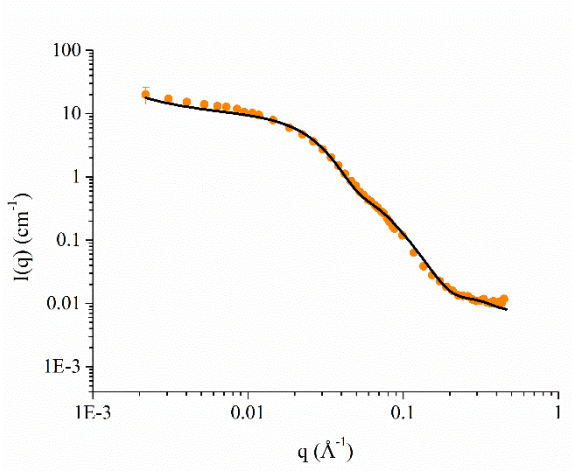

Figure 9 SANS profile of SPIONs/HSA upon removal of protein excess. Best fitting curve is also shown in black.

For comparison the parameters obtained from the fitting of SPIONs/HSA, SPIONs and HSA are reported in Table 1. What emerges is that the core features are not affected by addition of HSA, as expected, with similar radius and *sld* values obtained. Significant differences arise when the shells of the two systems are compared: the shell *sld* value is one order of magnitude higher in the case SPIONs/HSA with respect to SPIONs; moreover, in the case of SPIONs/HSA the shell is thicker than that of SPIONs (48 *vs* 36 Å, respectively). The thicker shell and the *sld* value are comparable with that of HSA suggesting the presence of HSA on the NP surface.

The overall radius of SPIONs/HSA cannot be immediately interpreted as the sum of SPION and HSA radii. The last apparent discrepancy may be due to i) HSA penetration within NP coating; ii) removal of the external 18LPC layer; or iii) the result of an incomplete protein coating. As for the first point, such a drastic change in the HSA environment should have resulted in a much more marked change of protein emission wavelength with respect to what was observed in fluorescence spectra of SPIONs/HSA even at high HSA:SPION. A similar consideration could be done in the second case, too: displacement of 18LPC would leave SPIONs exposing the hydrophobic tails of oleic acid/oleylamine that would then be free to interact with HSA. HSA is a lipid binding protein with many sites devoted to lipid recognition, but also in this case the fluorescence spectra of the HSA/SPIONs should present a blue shift at least comparable to that observed for the 18LPC/HSA system (Figure S2). Thus, considering also the R_H value determined by DLS, which differs from the radius obtained by SANS for taking into account also the hydration shell, we think that in the SPIONs/HSA system protein molecules are bound on the NP coating forming an incomplete protein corona. The quite high polydispersity of SPION/HSA radii may be a further index of incomplete coating.

It is interesting to note that formation of an incomplete protein shell may be the driving force for NP/protein aggregation, which was proved to happen by both DLS and SANS results. In this respect, this likely represents a different aggregation mechanism with respect to SPIONs/HTF system where depletion effect seems preponderant.

Table 1 Structural parameters for SPIONs/HSA in comparison with those of isolated HSA and SPIONs as determined by fitting of SANS data

	SPIONs/HSA	**SPIONs***	**HSA**
Model	Core-shell sphere + power law	Core-shell sphere	Ellipsoid
Core radius r_{core} (Å)	25 ± 2	27 ± 2	
***sld* core ρ_{core} x 10^{-6} (Å^{-2})**	6.9	6.9	
Shell thickness d (Å)	48 ± 1	36 ± 1	
***sld* shell ρ_{shell} x 10^{-6} (Å^{-2})**	4 ± 1	0.62	
***sld* ρ x 10^{-6} (Å^{-2})**			1.86
Minor radius a (Å)			11 ± 0.1
Major radius b (Å)			49 ± 0.5
Power law	-1.5		

* as reported in Luchini *et al*., Phys. Chem., Chem. Phys., 18, 18441 (2016)

Based on fluorescence, DLS and SANS results it is possible to propose a HSA binding mode. HSA has an almost triangular shape, with 8 nm edges and 3.5 nm thickness (Figure 10A). The only tryptophan residue (marked in red in Figure 10A) is located in the middle of one of the HSA faces and is quite exposed to the solvent. The NP quenching effect, as well as the blue shift of the tryptophan emission maximum, suggests a close interaction between the nanoparticle and the tryptophan. At the same time DLS and SANS indicate the presence of a thin protein layer, which is not compatible with HSA binding with any of its 8 nm edges, as observed in the case of some Au/Ag NPs[41b] and Au NPS.[42] Thus we can infer that HSA binds SPIONs in a "side on" mode,[20] similarly to what found in

the case of polymer coated FePt NPs.[43] At the same time we can rule out the formation of protein dimers on NP surface, as suggested for BSA on Al_2O_3 NPs.[44]

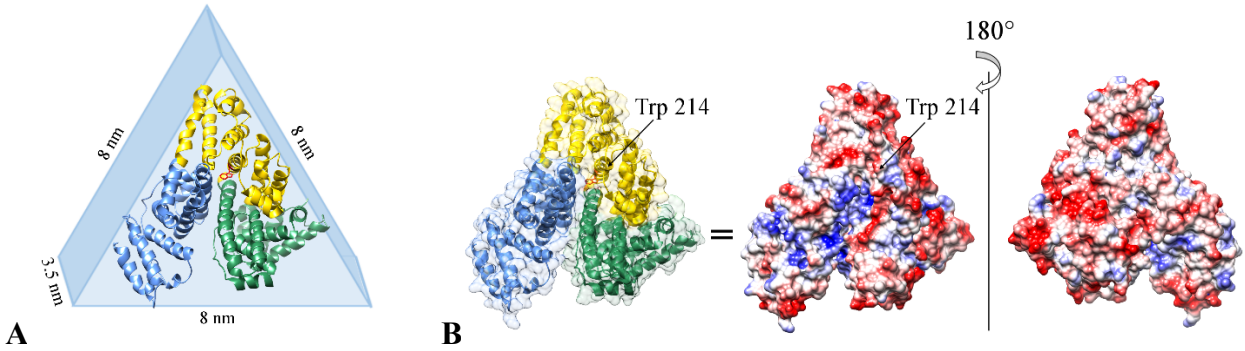

Figure 10 A) Crystal structure and scheme of HSA with different domains highlighted in different colours. The only Trp is marked in red. B) HSA electrostatic surface representation at pH 7: positive charges are coloured in blue, negative ones in red, neutral zone in light grey. The position of Trp is explicitly shown.

This hypothesis well justifies the zeta potential results too. Indeed, HSA is characterized by the presence of differently charged patches on its surface. On the Trp-face, numerous positive patches may drive the binding via Coulomb interactions[43] with the slightly negatively charged SPIONs, by leaving the opposite HSA face exposed to the solvent, which is less charged (Figure 10B).

We can tentatively evaluate the number of HSA molecules bound on the NP surface (N) considering dimensions of SPIONs and HSA/SPIONs (Figure S10) as determined by DLS or SANS as

$$N = \frac{{}^{4}/_{3}\pi\,(r^3_{HSA/SPIONs} - r^3_{SPIONs})}{V_{HSA}} \qquad \text{Eq. 4}$$

We find $N \approx 7$ molecules in both cases, which is in reasonable agreement with results obtained in the case of BSA and different superparamagnetic nanoparticles with similar dimensions.[20] At the same time, this value is significantly lower than the maximum number of HSA molecules required to form a monolayer on the NP through a side on binding mode that is about 20 (calculated by dividing the surface area of an individual NP by the triangular area of one HSA molecule[45]), strengthening the hypothesis of incomplete coverage.

Interaction of SPIONs/HSA aggregates with model membranes

Overall, the characterization of SPIONs/HSA system points toward the presence of NP with a slightly different coating, including an incomplete HSA layer strongly adsorbed on the 18LPC. This

modification may affect behaviour of NPs *in vivo*, particularly their interaction with cells and internalization pathways. Since the first step of NP entry into cells is determined by their interaction with the cell membrane,[46] we analysed SPIONs/HSA interaction with model membranes by means of neutron reflectivity.[47] NP membrane activity can be predicted by observing the interactions with solid supported lipid bilayers, composed of homogeneous fluid lipid mixtures, without raft-like domains or embedded membrane proteins.[46] Thus, we studied HSA and SPIONs/HSA interaction with lipid bilayers formed by 1-palmitoyl-2-oleoyl-*sn*-glycero-3-phosphocholine (POPC), 1-palmitoyl-2-oleoyl-*sn*-glycero-3-phospho-(1'-rac-glycerol) (POPG) and cholesterol (Chol) at different molar ratios, namely POPC/POPG/Chol 72/8/20 and 56/4/40. POPC is a zwitterionic lipid, while POPG was used to confer a slight negative charge to lipid bilayers thus better mimicking biological membranes.[48] Cholesterol was also added as it is an important component of cellular membranes, which regulates their fluidity and packing and takes part in several biological processes. Data were fit according to a box-model[35] where the silicon block, the thin solvent layer interposed between it and the supported bilayer, the inner headgroups, the hydrophobic chains and the outer headgroups of the bilayer, each of which represents a box. In the case of systems containing either HSA, SPIONs/HSA or SPIONs an additional layer was included (Figure S11). Each box was characterized in terms of thickness, *sld*, solvent content and roughness. Structural parameters of the silicon block were kept fixed and equal to those obtained from the analysis of the bare surfaces.

As an example, in Figure 11 the NR profiles, both experimental data and fitting curves, of the POPC/POPG/Chol 72/8/20 bilayer alone and in the presence of either HSA or SPIONs/HSA in D_2O are reported (NR profiles in different contrast media are reported in Figure S12).

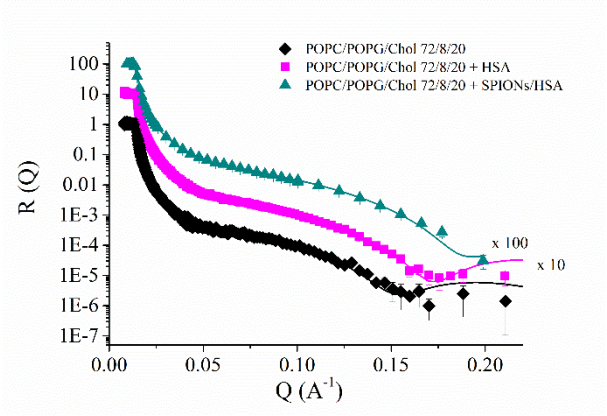

Figure 11 NR profiles for POPC/POPG/Chol 72/8/20 bilayer before and after injection of either SPIONs/HSA or HSA in D_2O. Best fitting curves are also reported.

Parameters deriving from fitting are summarized in Table 2 compared to those reported for the same lipid bilayer in the presence of SPIONs.[48] These results suggest the adhesion of both SPIONs/HSA and HSA on the surface of the bilayers, even if the high solvent content indicates that only a small fraction is indeed present on the bilayer surface, while most of them are likely removed by washing with solvent.

Table 2 Comparison among structural parameters of POPC/POPG/Chol 72/8/20 lipid bilayer before and after injection of SPIONs/HSA, HSA alone and SPIONs alone. Errors as derived from fitting are reported.

	Thickness (Å)	***sld* x 10^{-6} ($Å^{-2}$)**	**Solvent fraction**	**Roughness (Å)**
POPC/POPG/Chol 72/8/20				
Inner Headgroups	7 ± 1	1.65 ± 0.02	0.45 ± 0.01	2 ± 1
Acyl chains	34 ± 1	-0.15 ± 0.02	0.010 ± 0.001	6 ± 1
Outer Headgroups	7 ± 1	1.65 ± 0.02	0.75 ± 0.05	2 ± 1
POPC/POPG/Chol 72/8/20 + SPIONs/HSA				
Inner Headgroups	6.7 ± 0.3	1.7 ± 0.1	0.27 ± 0.02	2 ± 1
Acyl chains	32 ± 1	-0.15 ± 0.02	0.025 ± 0.002	3 ± 1
Outer Headgroups	10 ± 1	1.50 ± 0.04	0.62 ± 0.04	2 ± 1
SPIONs/HSA	80 ± 2	2.65 ± 0.06	0.86 ± 0.02	40 ± 5
POPC/POPG/Chol 72/8/20 + HSA				
Inner Headgroups	6 ± 1	1.60 ± 0.02	0.40 ± 0.05	4 ± 2
Acyl chains	31 ± 1	-0.15 ± 0.02	0.21 ± 0.01	3 ± 1
Outer Headgroups	9 ± 1	1.40 ± 0.02	0.45 ± 0.01	4 ± 1
HSA	15 ± 4	5.00± 0.02	0.90 ± 0.02	5 ± 2
POPC/POPG/Chol 72/8/20 + SPIONs*				
Inner Headgroups	7 ± 1*	1.60 ± 0.02*	0.32 ± 0.02*	5 ± 1*
Acyl chains	33 ± 1*	-0.15 ± 0.02*	0.09 ± 0.01*	2 ± 1*
Outer Headgroups	7 ± 1*	1.44 ± 0.02*	0.45 ± 0.03*	7 ± 2*
SPIONs	65 ± 5*	1.1 ± 0.2*	0.90 ±0.01*	25 ± 5*

* as reported in Luchini *et al.*[48]

In further details, SPIONs/HSA binding does not affect bilayer features, with a total bilayer thickness of about 49 Å, very similar to the 48 Å of the isolated bilayer. The interaction with HSA does not induce any significant change in the bilayer thickness (46 Å) but, on the other hand, affects the solvent content, which increases with respect to the pure bilayer, particularly in the acyl chain region This finding may suggest that isolated proteins could slightly enhance membrane permeability. In this respect, it should be recalled that the model membranes used have a slight negative charge and HSA presents positive residues on its surface, thus an electrostatic interaction between them may occur. On the other hand, these positive protein patches are shielded in the SPIONs/HSA assemblies (see above) and this may explain the different behaviour of the two systems.

Results obtained in the case of POPC/POPG/Chol 56/4/40 generally agree with those illustrated for the POPC/POPG/Chol 72/8/20 system (see Supplementary Materials, Table S1 and Figures S13 and S14).

Overall, NR analysis clearly shows that interaction with SPIONs/HSA does not significantly alter the membrane properties: specifically, they do not break the bilayer or induce the formation of pores. Similar results obtained with SPIONs[48] pointed towards their biocompatibility and the present data reinforce this idea, since it should be recalled that NPs rarely, if ever, retain their properties when placed in a biological context and most likely what meet membranes are NPs coated by serum proteins, such as HSA.

Conclusions

Here we show that SPIONs covered by a double layer of oleic acid/oleylamine and 18LPC are able to interact with both the abundant human plasma proteins HSA and HTF, but the kind and strength of interaction is crucially dependent on the nature of the protein.

In the case of HTF the interaction is rather weak. Fluorescence quenching experiments indicate in the HTF/SPIONs system the coexistence of static and dynamic quenching, DLS analysis confirms the interaction between SPIONs and HTF resulting in some sort of NP-proteins aggregates, which dimensions range from $R_H \approx 20$ and 40 nm, but the formation of a stable complex is ruled out by the analysis of washed samples where no CD signal due to the protein is detectable. Notably no effect of SPIONs on HTF secondary and tertiary structure is observed, differently to what found for bare and PVA-coated SPIONs with similar dimensions, which cause irreversible changes of the protein conformation, even if it should be noted that in that case holo-transferrin was used.[49]

On the other hand, in the case of HSA a tight NP-protein complex forms, characterized by a binding constant of ~10^8 M^{-1} and a well defined geometry of interaction, i.e. HSA binds in a side on mode. It is interesting that HSA seems able to form both a hard and a soft corona on the SPION surface: indeed in the presence of protein excess we observe a population of $R_H \approx 25$ nm in DLS spectra coexisting with the isolated HSA population. We can suggest that multiple protein layers can form, but when a threshold is reached no further HSA binding occurs and protein molecules remain unbound in solution. Upon extensive washing of protein excess, only SPION/HSA complexes with $R_H \approx 10$ nm are observed, an indication that loosely bound protein molecules are removed by the washing procedure together with unbound ones.

The presence of hydrophobic moieties as well as hydrophilic negatively charged groups are the basic structural requirements for ligand binding to HSA.[50] The peculiar coating of our SPIONs, bearing zwitterionic amphiphiles that at physiological pH are characterized by a slightly negative charge, as determined by electrophoretic light scattering, may justify the strong binding of HSA. Furthermore, the driving force for the interaction may be envisaged also in the slight change of HSA structure in the presence of NPs, as highlighted by CD spectra. Indeed in the case of binding of the analogous protein BSA to negatively charged silica particles, the slight change of protein structure, with an increase of unordered content, was suggested to be the driving force for the binding.[51] Indeed, this kind of structural reorganization may take place driven by favourable protein–surface interactions and involves an entropy gain due to the loss of ordered secondary structure inside the protein plus the release of counter ions or solvation molecules.[52]

Usually strong protein binding to flat surfaces of large NP was suggested as a cause of protein structure modification and even unfolding.[53] Unfolded or misfolded proteins not only are devoid of their normal biological activity, but often aggregate and/or interact improperly with other cellular components, with the result of impairing cell viability and eventually even causing cell death.[53a] In this respect the small dimension of our SPIONs can be called into play for their biocompatibility, at least with respect to interactions with proteins: indeed in the presence of a strong binding between a quite large protein such as HSA and the NP surface, no significant conformational change is detected for the protein.

HSA-covered SPIONs are able to interact with and adhere to the surface of lipid bilayers used as membrane models without removing lipids nor affecting the membrane structure, similarly to the reference SPIONs.[48] Considering the potential application of SPIONs as MRI contrast agents, they should be able to interact with the cells of a target tissue without compromising their life and this interaction should occur even in the presence of the protein corona very likely formed *in vivo*.

Finally, the apparent preferential binding of HSA with respect to HTF, taking into account the higher HSA concentration in human plasma (40 *vs* 2.8 mg ml^{-1} for HSA and HTF, respectively)[54] may have important biological consequences. In fact, a HTF receptor is often overexpressed on the surface of malignant cells,[25] thus NP coverage by HTF may significantly affect the fate of the NP *in vivo*. On the other hand, the HSA layer tightly bound to the SPIONs could be exploited for further functionalization of NPs, by taking advantage of the carrier properties of this protein, which have often been used to deliver drugs and diagnostic probes.[55] Moreover, SPIONs bearing a protein corona enriched in albumin might better escape the immune system[56] and it has been also shown that pre-coating SPIONs with albumin and lipoproteins can help them to cross biological barriers, such as the blood–brain barrier.[57]

Altogether, present findings reinforce the idea of our amphiphiles-coated SPIONs as a biocompatible nanodevice for biomedical applications.

Acknowledgements

This work was supported by Regional Operational Programme (P.O.R.) Campania, "Development of novel therapeutic approaches for treatment-resistant neoplastic diseases" (acronym: SATIN).

This work is based upon experiments performed at the KWS-2 instrument (proposal number 12856) and MARIA instrument (proposal number 12983) operated by JCNS at the Heinz Maier-Leibnitz Zentrum (MLZ), Garching, Germany and at the D17 reflectometer operated by the ILL, Grenoble, France (doi:10.5291/ILL-DATA.8-02-801). The authors gratefully acknowledge the financial support provided by JCNS to perform the neutron scattering measurements at the Heinz Maier-Leibnitz Zentrum (MLZ), Garching, Germany. This work benefited from the use of the SasView application, originally developed under NSF Award DMR-0520547. SasView also contains code developed with funding from the EU Horizon 2020 programme under the SINE2020 project Grant No 654000.

Conflicts of interest

There are no conflicts to declare.

References

1. (a) Jeevanandam, J.; Barhoum, A.; Chan, Y. S.; Dufresne, A.; Danquah, M. K., Review on nanoparticles and nanostructured materials: history, sources, toxicity and regulations. *Beilstein J Nanotech* **2018,** *9*, 1050-1074; (b) Conde, J.; Dias, J. T.; Grazu, V.; Moros, M.; Baptista, P. V.; de la Fuente, J. M., Revisiting 30 years of biofunctionalization and surface chemistry of inorganic nanoparticles for nanomedicine. *Front Chem* **2014,** *2*.
2. Parveen, R.; Shamsi, T. N.; Fatima, S., Nanoparticles-protein interaction: Role in protein aggregation and clinical implications. *Int J Biol Macromol* **2017,** *94*, 386-395.
3. Pomerantseva, E.; Bonaccorso, F.; Feng, X.; Cui, Y.; Gogotsi, Y., Energy storage: The future enabled by nanomaterials. *Science* **2019,** *366* (6468).
4. Rani, A.; Reddy, R.; Sharma, U.; Mukherjee, P.; Mishra, P.; Kuila, A.; Sim, L. C.; Saravanan, P., A review on the progress of nanostructure materials for energy harnessing and environmental remediation. *J Nanostructure Chem* **2018,** *8* (3), 255-291.
5. Subramanian, V.; Lee, T., Nanotechnology-based flexible electronics. *Nanotechnology* **2012,** *23* (34).
6. Chen, M. J.; Yang, W. T.; Yin, M. Z., Synthesis and Applications of Nanoparticles in Biology. *Prog Chem* **2012,** *24* (12), 2403-2414.
7. (a) Daraee, H.; Eatemadi, A.; Abbasi, E.; Fekri Aval, S.; Kouhi, M.; Akbarzadeh, A., Application of gold nanoparticles in biomedical and drug delivery. *Artificial cells, nanomedicine, and biotechnology* **2016,** *44* (1), 410-22; (b) Li, X.; Wei, J.; Aifantis, K. E.; Fan, Y.; Feng, Q.; Cui, F. Z.; Watari, F., Current investigations into magnetic nanoparticles for biomedical applications. *Journal of biomedical materials research. Part A* **2016,** *104* (5), 1285-96; (c) Rudramurthy, G. R.; Swamy, M. K., Potential applications of engineered nanoparticles in medicine and biology: an update. *J Biol Inorg Chem* **2018,** *23* (8), 1185-1204.
8. Ghazanfari, M. R.; Kashefi, M.; Shams, S. F.; Jaafari, M. R., Perspective of Fe3O4 Nanoparticles Role in Biomedical Applications. *Biochemistry research international* **2016,** *2016*, 7840161.
9. (a) Fleischer, C. C.; Payne, C. K., Nanoparticle-cell interactions: molecular structure of the protein corona and cellular outcomes. *Accounts of chemical research* **2014,** *47* (8), 2651-9; (b) Rodriguez-Quijada, C.; Sanchez-Purra, M.; de Puig, H.; Hamad-Schifferli, K., Physical Properties of Biomolecules at the Nanomaterial Interface. *J Phys Chem B* **2018,** *122* (11), 2827-2840.
10. (a) Kandasamy, G.; Maity, D., Recent advances in superparamagnetic iron oxide nanoparticles (SPIONs) for in vitro and in vivo cancer nanotheranostics. *International journal of pharmaceutics* **2015,** *496* (2), 191-218; (b) Li, L.; Jiang, W.; Luo, K.; Song, H.; Lan, F.; Wu, Y.; Gu, Z., Superparamagnetic iron oxide nanoparticles as MRI contrast agents for non-invasive stem cell labeling and tracking. *Theranostics* **2013,** *3* (8), 595-615; (c) Yoffe, S.; Leshuk, T.; Everett, P.; Gu, F., Superparamagnetic iron oxide nanoparticles (SPIONs): synthesis and surface modification techniques for use with MRI and other biomedical applications. *Current pharmaceutical design* **2013,** *19* (3), 493-509; (d) Zhu, L.; Zhou, Z.; Mao, H.; Yang, L., Magnetic nanoparticles for precision oncology: theranostic magnetic iron oxide nanoparticles for image-guided and targeted cancer therapy. *Nanomedicine* **2017,** *12* (1), 73-87.
11. Santhosh, P. B.; Ulrih, N. P., Multifunctional superparamagnetic iron oxide nanoparticles: promising tools in cancer theranostics. *Cancer letters* **2013,** *336* (1), 8-17.
12. Mendozza, M.; Montis, C.; Caselli, L.; Wolf, M.; Baglioni, P.; Berti, D., On the thermotropic and magnetotropic phase behavior of lipid liquid crystals containing magnetic nanoparticles. *Nanoscale* **2018,** *10* (7), 3480-3488.
13. Kim, J.; Piao, Y.; Hyeon, T., Multifunctional nanostructured materials for multimodal imaging, and simultaneous imaging and therapy. *Chem Soc Rev* **2009,** *38* (2), 372-390.
14. Gagner, J. E.; Shrivastava, S.; Qian, X.; Dordick, J. S.; Siegel, R. W., Engineering Nanomaterials for Biomedical Applications Requires Understanding the Nano-Bio Interface: A Perspective. *J Phys Chem Lett* **2012,** *3* (21), 3149-3158.
15. Guerrini, L.; Alvarez-Puebla, R. A.; Pazos-Perez, N., Surface Modifications of Nanoparticles for Stability in Biological Fluids. *Materials* **2018,** *11* (7).
16. (a) Luchini, A.; Vitiello, G.; Rossi, F.; De Ballesteros, O. R.; Radulescu, A.; D'Errico, G.; Montesarchio, D.; Fernandez, C. D.; Paduano, L., Developing functionalized Fe3O4-Au nanoparticles: a physico-chemical

insight. *Phys Chem Chem Phys* **2015,** *17* (8), 6087-6097; (b) Luchini, A.; Heenan, R. K.; Paduano, L.; Vitiello, G., Functionalized SPIONs: the surfactant nature modulates the self-assembly and cluster formation. *Phys Chem Chem Phys* **2016,** *18* (27), 18441-18449.
17. Luchini, A.; D'Errico, G.; Leone, S.; Vaezi, Z.; Bortolotti, A.; Stella, L.; Vitiello, G.; Paduano, L., Structural organization of lipid-functionalized-Au nanoparticles. *Colloid Surface B* **2018,** *168*, 2-9.
18. (a) Luchini, A.; Irace, C.; Santamaria, R.; Montesarchio, D.; Heenan, R. K.; Szekely, N.; Flori, A.; Menichetti, L.; Paduano, L., Phosphocholine-decorated superparamagnetic iron oxide nanoparticles: defining the structure and probing in vivo applications. *Nanoscale* **2016,** *8* (19), 10078-86; (b) Riccardi, C.; Musumeci, D.; Capuozzo, A.; Irace, C.; King, S.; Krauss, I. R.; Paduano, L.; Montesarchio, D., "Dressing up" an Old Drug: An Aminoacyl Lipid for the Functionalization of Ru(III)-Based Anticancer Agents. *Acs Biomater Sci Eng* **2018,** *4* (1), 163-174.
19. Riccardi, C.; Musumeci, D.; Krauss, I. R.; Piccolo, M.; Irace, C.; Paduano, L.; Montesarchio, D., Exploring the conformational behaviour and aggregation properties of lipid-conjugated AS1411 aptamers. *Int J Biol Macromol* **2018,** *118*, 1384-1399.
20. Yu, S. M.; Peralvarez-Marin, A.; Minelli, C.; Faraudo, J.; Roig, A.; Laromaine, A., Albumin-coated SPIONs: an experimental and theoretical evaluation of protein conformation, binding affinity and competition with serum proteins. *Nanoscale* **2016,** *8* (30), 14393-14405.
21. (a) Zhang, X. N.; Zhang, J. T.; Zhang, F.; Yu, S. N., Probing the binding affinity of plasma proteins adsorbed on Au nanoparticles. *Nanoscale* **2017,** *9* (14), 4787-4792; (b) Monopoli, M. P.; Aberg, C.; Salvati, A.; Dawson, K. A., Biomolecular coronas provide the biological identity of nanosized materials. *Nat Nanotechnol* **2012,** *7* (12), 779-786; (c) Monopoli, M. P.; Bombelli, F. B.; Dawson, K. A., NANOBIOTECHNOLOGY Nanoparticle coronas take shape. *Nat Nanotechnol* **2011,** *6* (1), 11-12; (d) Monopoli, M. P.; Walczyk, D.; Campbell, A.; Elia, G.; Lynch, I.; Bombelli, F. B.; Dawson, K. A., Physical-Chemical Aspects of Protein Corona: Relevance to in Vitro and in Vivo Biological Impacts of Nanoparticles. *J Am Chem Soc* **2011,** *133* (8), 2525-2534.
22. Dominguez-Medina, S.; Kisley, L.; Tauzin, L. J.; Hoggard, A.; Shuang, B.; Indrasekara, A. S. D. S.; Chen, S. S.; Wang, L. Y.; Derry, P. J.; Liopo, A.; Zubarev, E. R.; Landes, C. F.; Link, S., Adsorption and Unfolding of a Single Protein Triggers Nanoparticle Aggregation. *Acs Nano* **2016,** *10* (2), 2103-2112.
23. Saptarshi, S. R.; Duschl, A.; Lopata, A. L., Interaction of nanoparticles with proteins: relation to bio-reactivity of the nanoparticle. *J Nanobiotechnol* **2013,** *11*.
24. (a) Kendall, M.; Ding, P.; Kendall, K., Particle and nanoparticle interactions with fibrinogen: the importance of aggregation in nanotoxicology. *Nanotoxicology* **2011,** *5* (1), 55-65; (b) Wolfram, J.; Yang, Y.; Shen, J. L.; Moten, A.; Chen, C. Y.; Shen, H. F.; Ferrari, M.; Zhao, Y. L., The nano-plasma interface: Implications of the protein corona. *Colloid Surface B* **2014,** *124*, 17-24; (c) Zhu, J.; Sun, Z.; Li, J. J.; Zhao, J. W., Bovine Serum Albumins (BSA) Induced Aggregation and Separation of Gold Colloid Nanoparticles. *J Nanosci Nanotechno* **2012,** *12* (3), 2206-2211.
25. Salvati, A.; Pitek, A. S.; Monopoli, M. P.; Prapainop, K.; Bombelli, F. B.; Hristov, D. R.; Kelly, P. M.; Aberg, C.; Mahon, E.; Dawson, K. A., Transferrin-functionalized nanoparticles lose their targeting capabilities when a biomolecule corona adsorbs on the surface. *Nat Nanotechnol* **2013,** *8* (2), 137-143.
26. Kumar, S.; Yadav, I.; Aswal, V. K.; Kohlbrecher, J., Structure and Interaction of Nanoparticle-Protein Complexes. *Langmuir : the ACS journal of surfaces and colloids* **2018,** *34* (20), 5679-5695.
27. Pfeiffer, T.; De Nicola, A.; Montis, C.; Carla, F.; van der Vegt, N. F. A.; Berti, D.; Milano, G., Nanoparticles at Biomimetic Interfaces: Combined Experimental and Simulation Study on Charged Gold Nanoparticles/Lipid Bilayer Interfaces. *J Phys Chem Lett* **2019,** *10* (2), 129-137.
28. Ling, D. S.; Hyeon, T., Chemical Design of Biocompatible Iron Oxide Nanoparticles for Medical Applications. *Small* **2013,** *9* (9-10), 1450-1466.
29. Paul, B. K.; Guchhait, N., A spectral deciphering of the binding interaction of an intramolecular charge transfer fluorescence probe with a cationic protein: thermodynamic analysis of the binding phenomenon combined with blind docking study. *Photoch Photobio Sci* **2011,** *10* (6), 980-991.
30. Chi, Z. X.; Liu, R. T.; Teng, Y.; Fang, X. Y.; Gao, C. Z., Binding of Oxytetracycline to Bovine Serum Albumin: Spectroscopic and Molecular Modeling Investigations. *J Agr Food Chem* **2010,** *58* (18), 10262-10269.

31. Lomakin, A.; Teplow, D. B.; Benedek, G. B., Quasielastic Light Scattering for Protein Assembly Studies. In *Amyloid Proteins: Methods And Protocols*, Sigurdsson, E. M., Ed. Humana Press: Totowa *New Jearsey(2005; Vol. 299.
32. (a) Houston, J. E.; Brandl, G.; Drochner, M.; Kemmerling, G.; Engels, R.; Papagiannopoulos, A.; Sarter, M.; Stadler, A.; Radulescu, A., The high-intensity option of the SANS diffractometer KWS-2 at JCNS - characterization and performance of the new multi-megahertz detection system. *J Appl Crystallogr* **2018,** *51*, 323-336; (b) Radulescu, A.; Pipich, V.; Frielinghaus, H.; Appavou, M. S., KWS-2, the high intensity/wide Q-range small-angle neutron diffractometer for soft-matter and biology at FRM II. *J Phys Conf Ser* **2012,** *351*; (c) Radulescu, A.; Szekely, N. K.; Polachowski, S.; Leyendecker, M.; Amann, M.; Buitenhuis, J.; Drochner, M.; Engels, R.; Hanslik, R.; Kemmerling, G.; Lindner, P.; Papagiannopoulos, A.; Pipich, V.; Willner, L.; Frielinghaus, H.; Richter, D., Tuning the instrument resolution using chopper and time of flight at the small-angle neutron scattering diffractometer KWS-2. *J Appl Crystallogr* **2015,** *48*, 1849-1859.
33. Mattauch, S.; Koutsioubas, A.; Rucker, U.; Korolkov, D.; Fracassi, V.; Daemen, J.; Schmitz, R.; Bussmann, K.; Suxdorf, F.; Wagener, M.; Kammerling, P.; Kleines, H.; Fleischhauer-Fuss, L.; Bednareck, M.; Ossoviy, V.; Nebel, A.; Stronciwilk, P.; Staringer, S.; Godel, M.; Richter, A.; Kusche, H.; Kohnke, T.; Ioffe, A.; Babcock, E.; Salhi, Z.; Bruckel, T., The high-intensity reflectometer of the Julich Centre for Neutron Science: MARIA. *J Appl Crystallogr* **2018,** *51*, 646-654.
34. (a) Cubitt, R.; Fragneto, G., D17: the new reflectometer at the ILL. *Appl Phys a-Mater* **2002,** *74*, S329-S331; (b) Saerbeck, T.; Cubitt, R.; Wildes, A.; Manzin, G.; Andersen, K. H.; Gutfreund, P., Recent upgrades of the neutron reflectometer D17 at ILL. *J Appl Crystallogr* **2018,** *51*, 249-256.
35. Gerelli, Y., Aurore: new software for neutron reflectivity data analysis. *Journal of applied crystallography* **2016,** *49* (1), 330-339.
36. Wally, J.; Halbrooks, P. J.; Vonrhein, C.; Rould, M. A.; Everse, S. J.; Mason, A. B.; Buchanan, S. K., The crystal structure of iron-free human serum transferrin provides insight into inter-lobe communication and receptor binding. *J Biol Chem* **2006,** *281* (34), 24934-24944.
37. Amiri, M.; Jankeje, K.; Albani, J. R., Origin of Fluorescence Lifetimes in Human Serum Albumin. Studies on Native and Denatured Protein. *J Fluoresc* **2010,** *20* (3), 651-656.
38. (a) Huang, D. P.; Geng, F.; Liu, Y. H.; Wang, X. Q.; Jiao, J. J.; Yu, L., Biomimetic interactions of proteins with functionalized cadmium sulfide quantum dots. *Colloid Surface A* **2011,** *392* (1), 191-197; (b) Lakowicz, J. R., *Principles of fluorescence spectroscopy*. Plenum Press: New York, 1983; p xiv, 496 p.
39. Yang, Q. Q.; Liang, J. G.; Han, H. Y., Probing the Interaction of Magnetic Iron Oxide Nanoparticles with Bovine Serum Albumin by Spectroscopic Techniques. *J Phys Chem B* **2009,** *113* (30), 10454-10458.
40. Treuel, L.; Brandholt, S.; Maffre, P.; Wiegele, S.; Shang, L.; Nienhaus, G. U., Impact of Protein Modification on the Protein Corona on Nanoparticles and Nanoparticle-Cell Interactions. *Acs Nano* **2014,** *8* (1), 503-513.
41. (a) Dewald, I.; Isakin, O.; Schubert, J.; Kraus, T.; Chanana, M., Protein Identity and Environmental Parameters Determine the Final Physicochemical Properties of Protein-Coated Metal Nanoparticles. *J Phys Chem C* **2015,** *119* (45), 25482-25492; (b) Sharma, A. S.; Ilanchelian, M., Comprehensive Multispectroscopic Analysis on the Interaction and Corona Formation of Human Serum Albumin with Gold/Silver Alloy Nanoparticles. *J Phys Chem B* **2015,** *119* (30), 9461-9476; (c) Goy-Lopez, S.; Juarez, J.; Alatorre-Meda, M.; Casals, E.; Puntes, V. F.; Taboada, P.; Mosquera, V., Physicochemical Characteristics of Protein-NP Bioconjugates: The Role of Particle Curvature and Solution Conditions on Human Serum Albumin Conformation and Fibrillogenesis Inhibition. *Langmuir : the ACS journal of surfaces and colloids* **2012,** *28* (24), 9113-9126.
42. Miclaus, T.; Bochenkov, V. E.; Ogaki, R.; Howard, K. A.; Sutherland, D. S., Spatial Mapping and Quantification of Soft and Hard Protein Coronas at Silver Nanocubes. *Nano Lett* **2014,** *14* (4), 2086-2093.
43. Mahmoudi, M.; Abdelmonem, A. M.; Behzadi, S.; Clement, J. H.; Dutz, S.; Ejtehadi, M. R.; Hartmann, R.; Kantner, K.; Linne, U.; Maffre, P.; Metzler, S.; Moghadam, M. K.; Pfeiffer, C.; Rezaei, M.; Ruiz-Lozano, P.; Serpooshan, V.; Shokrgozar, M. A.; Nienhaus, G. U.; Parak, W. J., Temperature: The "Ignored" Factor at the NanoBio Interface. *Acs Nano* **2013,** *7* (8), 6555-6562.

44. Rezwan, K.; Meier, L. P.; Rezwan, M.; Voros, J.; Textor, M.; Gauckler, L. J., Bovine serum albumin adsorption onto colloidal Al2O3 particles: A new model based on zeta potential and UV-vis measurements. *Langmuir : the ACS journal of surfaces and colloids* **2004,** *20* (23), 10055-10061.
45. Gebauer, J. S.; Malissek, M.; Simon, S.; Knauer, S. K.; Maskos, M.; Stauber, R. H.; Peukert, W.; Treuel, L., Impact of the Nanoparticle-Protein Corona on Colloidal Stability and Protein Structure. *Langmuir : the ACS journal of surfaces and colloids* **2012,** *28* (25), 9673-9679.
46. Montis, C.; Generini, V.; Boccalini, G.; Bergese, P.; Bani, D.; Berti, D., Model lipid bilayers mimic non-specific interactions of gold nanoparticles with macrophage plasma membranes. *J Colloid Interf Sci* **2018,** *516*, 284-294.
47. Lolicato, F.; Joly, L.; Martinez-Seara, H.; Fragneto, G.; Scoppola, E.; Baldelli Bombelli, F.; Vattulainen, I.; Akola, J.; Maccarini, M., The Role of Temperature and Lipid Charge on Intake/Uptake of Cationic Gold Nanoparticles into Lipid Bilayers. *Small* **2019,** *15* (23), e1805046.
48. Luchini, A.; Gerelli, Y.; Fragneto, G.; Nylander, T.; Palsson, G. K.; Appavou, M. S.; Paduano, L., Neutron Reflectometry reveals the interaction between functionalized SPIONs and the surface of lipid bilayers. *Colloid Surface B* **2017,** *151*, 76-87.
49. Mahmoudi, M.; Shokrgozar, M. A.; Sardari, S.; Moghadam, M. K.; Vali, H.; Laurent, S.; Stroeve, P., Irreversible changes in protein conformation due to interaction with superparamagnetic iron oxide nanoparticles. *Nanoscale* **2011,** *3* (3), 1127-1138.
50. Fasano, M.; Curry, S.; Terreno, E.; Galliano, M.; Fanali, G.; Narciso, P.; Notari, S.; Ascenzi, P., The extraordinary ligand binding properties of human serum albumin. *Iubmb Life* **2005,** *57* (12), 787-796.
51. Giacomelli, C. E.; Norde, W., The Adsorption-Desorption Cycle. Reversibility of the BSA-Silica System. *Journal of colloid and interface science* **2001,** *233* (2), 234-240.
52. Rabe, M.; Verdes, D.; Seeger, S., Understanding protein adsorption phenomena at solid surfaces. *Advances in colloid and interface science* **2011,** *162* (1-2), 87-106.
53. (a) Lacerda, S. H. D.; Park, J. J.; Meuse, C.; Pristinski, D.; Becker, M. L.; Karim, A.; Douglas, J. F., Interaction of Gold Nanoparticles with Common Human Blood Proteins. *Acs Nano* **2010,** *4* (1), 365-379; (b) Walkey, C. D.; Chan, W. C. W., Understanding and controlling the interaction of nanomaterials with proteins in a physiological environment. *Chem Soc Rev* **2012,** *41* (7), 2780-2799.
54. Sun, H. Z.; Li, H. Y.; Mason, A. B.; Woodworth, R. C.; Sadler, P. J., Competitive binding of bismuth to transferrin and albumin in aqueous solution and in blood plasma. *J Biol Chem* **2001,** *276* (12), 8829-8835.
55. (a) Karimi, M.; Bahrami, S.; Ravari, S. B.; Zangabad, P. S.; Mirshekari, H.; Bozorgomid, M.; Shahreza, S.; Sori, M.; Hamblin, M. R., Albumin nanostructures as advanced drug delivery systems. *Expert opinion on drug delivery* **2016,** *13* (11), 1609-1623; (b) Kudarha, R. R.; Sawant, K. K., Albumin based versatile multifunctional nanocarriers for cancer therapy: Fabrication, surface modification, multimodal therapeutics and imaging approaches. *Materials science & engineering. C, Materials for biological applications* **2017,** *81*, 607-626; (c) Lamichhane, S.; Lee, S., Albumin nanoscience: homing nanotechnology enabling targeted drug delivery and therapy. *Archives of pharmacal research* **2020,** *43* (1), 118-133.
56. Jedlovszky-Hajdu, A.; Bombelli, F. B.; Monopoli, M. P.; Tombacz, E.; Dawson, K. A., Surface coatings shape the protein corona of SPIONs with relevance to their application in vivo. *Langmuir : the ACS journal of surfaces and colloids* **2012,** *28* (42), 14983-91.
57. Zensi, A.; Begley, D.; Pontikis, C.; Legros, C.; Mihoreanu, L.; Buchel, C.; Kreuter, J., Human serum albumin nanoparticles modified with apolipoprotein A-I cross the blood-brain barrier and enter the rodent brain. *Journal of drug targeting* **2010,** *18* (10), 842-8.